Unconventional $S = 2$ alternating chain realized by a metal-radical hybrid-spin approach

H. Yamaguchi,[1] Y. Shinpuku,[1] Y. Kono,[2] S. Kittaka,[2] T. Sakakibara,[2] M. Hagiwara,[3] T. Kawakami,[4] K. Iwase,[1] T. Ono,[1] and Y. Hosokoshi[1]

[1]*Department of Physical Science, Osaka Prefecture University, Osaka 599-8531, Japan*

[2]*Institute for Solid State Physics, University of Tokyo, Chiba 277-8581, Japan*

[3]*Center for Advanced High Magnetic Field Science, Graduate School of Science, Osaka University, Osaka 560-0043, Japan*

[4]*Department of Chemistry, Osaka University, Osaka 560-0043, Japan*

(Received 12 February 2015; revised manuscript received 9 March 2016; published 29 March 2016)

We demonstrate an advanced spin-system design using a hybrid spin consisting of a strongly coupled metal ion and verdazyl radical. *Ab initio* calculation, magnetization, and ESR measurements evidenced the first realization of an $S = 2$ ferromagnetic-antiferromagnetic alternating chain with Ising anisotropy in a Mn-verdazyl complex $[Mn(hfac)_2] \cdot$ (*o*-Py-V) [hfac = 1,1,1,5,5,5-hexafluoroacetylacetonate; *o*-Py-V = 3-(2-pyridyl)-1,5-diphenylverdazyl]. Furthermore, we find an anomalous change in magnetization at 1/4 of the saturation value, which is probably a manifestation of the quantum nature of the system.

DOI: 10.1103/PhysRevB.93.115145

I. INTRODUCTION

Organic radicals have attracted considerable attention as next-generation spin sources for not only fundamental studies of magnetism but also application as radical-based batteries [1,2] or spintronic devices [3,4]. The diversity of molecular arrangements in organic-radical materials is expected to facilitate the design of magnetic materials. A large number of organic-radical materials have been synthesized in the past two decades since the discovery of the first organic ferromagnet [5] through the use of representative nitroxide-type radicals [6]. However, most of them have exhibited a simple stacking of planar molecules with a localized π-electron spin density, resulting in the formation of well-known one-dimensional (1D) spin systems, such as the $S = 1/2$ antiferromagnetic (AF) chain. To solve this problem, we have focused on the verdazyl radical, which can exhibit a delocalized π-electron spin density even in nonplanar molecular structures. The flexibility of the molecular orbitals in the verdazyl radical is expected to enable the tuning of intermolecular magnetic interactions through chemical modification. Recently, we established synthetic techniques for preparing high-quality verdazyl-radical crystals and demonstrated the tuning of magnetic interactions in a variety of unconventional spin systems [7–10].

In addition to magnetic interaction, two principal parameters are required for designing a magnetic material: spin size and magnetic anisotropy. Although polyradicals can produce $S > 1/2$ spin systems through strong intramolecular magnetic interactions, synthesis of such molecules requires many processes [6,11,12]. Furthermore, organic radicals are almost isotropic at experimental temperatures owing to the negligible spin-orbit couplings in light elements. One practical strategy for modulating both spin size and magnetic anisotropy is to combine radicals with transition-metal ions. Indeed, metal-radical complexes have mainly been reported thus far by using nitroxide-type radicals [13–15]. The principle motivation behind synthesizing these complexes has been to form high-dimensional ferromagnetic and ferrimagnetic materials by taking advantage of strong couplings via the coordination. The coordination chemistry of the verdazyl radical has also been under intense investigation [16,17] since the first complexes were reported in 1997 by Brook *et al.* [18]. Very recently, we succeeded in combining our verdazyl radicals with 3*d* transition metals to obtain single crystals of a molecular-based complex [19]. The strong intramolecular couplings in such molecular-based complexes can produce a metal-radical hybrid spin in low-temperature regions [20–22]. In the present study, we utilize this hybrid spin to introduce an $S > 1/2$ spin and magnetic anisotropy in verdazyl-radical materials.

Quantum spin systems provide various unique many-body phenomena. Haldane's prediction in 1983 [23] has stimulated experimental and theoretical studies focused on the qualitative difference between half-integer and integer spin Heisenberg AF chains. Subsequent investigations on $S = 1$ systems have established the presence of a Haldane gap in the integer spin case [24–27]. The ground state below the Haldane gap is well described as a valence-bond solid (VBS) [28,29], in which each integer spin is considered two half spins forming a singlet state between different sites. However, there are remarkably few examples of $S > 1$ 1D spin systems. The second-minimal integer spin, $S = 2$, has only several examples [30–35], and their quantum behavior still has not been clarified. The ground-state phase diagram on the $S = 2$ AF chain is discussed in several numerical works [36–43], in which various quantum phases appear in accordance with the combination of exchange interactions and magnetic anisotropy. Moreover, bond alternation in the $S = 2$ AF chain is expected to induce breaking of a hidden symmetry in the VBS state [44–46].

The VBS of an integer spin chain can be mapped onto the strong ferromagnetic (F) coupling limit of an F-AF alternating chain with half spin. Therefore, the $S = 1/2$ Heisenberg F-AF chain has been studied in relation to the Haldane state in the $S = 1$ Heisenberg AF chain [47–49]. Hida investigated the ground-state properties for various ratios of exchange constants [50–52]. The energy gap and string order parameter, which indicates hidden topological order specific to VBS, have finite values for all the ratios of exchange constants and change continuously from the $S = 1$ Haldane phase ($|J_F| \gg J_{AF}$) to the $S = 1/2$ AF dimer phase ($|J_F| \ll J_{AF}$). Thus, it is suggested that there is no discontinuous change in the ground state associated with a phase transition between two opposite

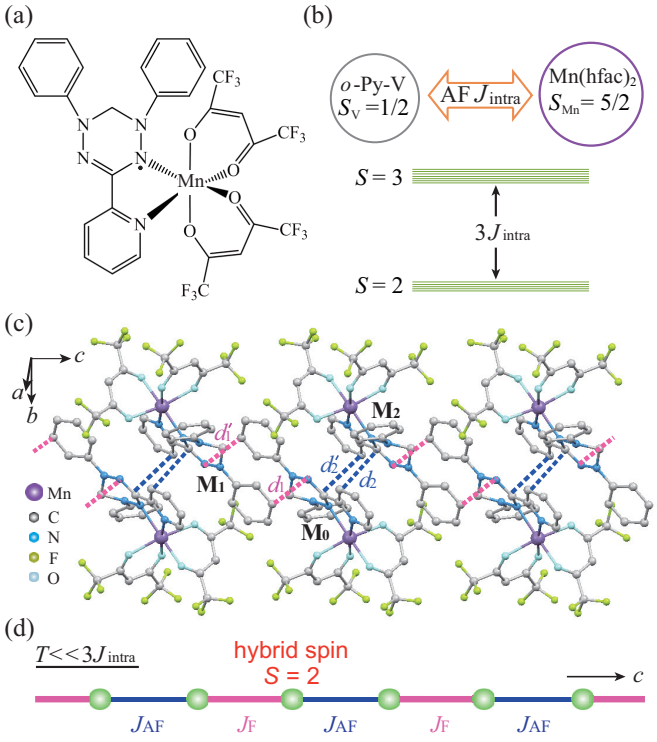

FIG. 1. (a) Molecular structure of $[Mn(hfac)_2]\cdot(o\text{-Py-V})$. (b) Schematic view of intramolecular interaction between spins on Mn^{2+} and verdazyl radical and resulting spin states. (c) Crystal structure forming an alternating chain along the c axis and (d) the corresponding spin model. Hydrogen atoms are omitted for clarity.

limiting cases. Accordingly, the ground-state properties of the present $S = 2$ F-AF alternating chain could be related to those of an $S = 4$ AF chain, even though the details of the exchange path slightly differ from those in the $S = 1/2$ case.

In this paper, we report a model compound of an $S = 2$ F-AF alternating chain with Ising anisotropy realized using a hybrid-spin approach. We have succeeded in synthesizing a Mn-verdazyl complex $[Mn(hfac)_2]\cdot(o\text{-Py-V})$, where hfac represents 1,1,1,5,5,5-hexafluoroacetylacetonate and *o*-Py-V stands for 3-(2-pyridyl)-1,5-diphenylverdazyl. The *ab initio* molecular orbital (MO) calculations and experimental measurements for this material evidenced the formation of the $S = 2$ F-AF alternating chain. The magnetic properties indicated remarkably anisotropic behavior, and on-site biaxial anisotropy was evaluated from the electron spin resonance (ESR) analysis. Furthermore, we observed an anomalous change in magnetization at 1/4 of the saturation value.

II. EXPERIMENT

The synthesis of $[Mn(hfac)_2]\cdot(o\text{-Py-V})$, whose molecular structure is shown in Fig. 1(a), was performed using a procedure similar to that for $[Zn(hfac)_2]\cdot(o\text{-Py-V})$ [19]. The recrystallization in acetonitrile yielded brown crystals. X-ray intensity data were collected using a Rigaku AFC-7R mercury CCD diffractometer and a Rigaku AFC-8R mercury CCD RA-micro7 diffractometer at 293 and 25 K, respectively, with graphite-monochromated Mo Kα radiation and Japan Thermal Engineering XR-HR10K. The structure was solved by a direct method using SIR2004 [53] and was refined with SHELXL97 [54]. The structural refinement was carried out using anisotropic and isotropic thermal parameters for the nonhydrogen atoms and the hydrogen atoms, respectively. All the hydrogen atoms were placed at the calculated ideal positions.

The magnetic susceptibility and magnetization curves were measured using a commercial superconducting quantum interference device (SQUID) magnetometer (MPMS-XL, Quantum Design) and a capacitive Faraday magnetometer with a dilution refrigerator down to about 70 mK. The experimental results were corrected for the diamagnetic contribution calculated by Pascal's method. The specific heat was measured using a handmade apparatus by a standard adiabatic heat-pulse method with a dilution refrigerator down to about 80 mK. The ESR measurements were performed utilizing a vector network analyzer (ABmm), a superconducting magnet (Oxford Instruments), and a homemade ESR cryostat at the Center for Advanced High Magnetic Field Science of Osaka University. All experiments were performed using single crystals with typical dimensions of $3.0\times1.0\times0.5$ mm.

Ab initio MO calculations were performed using the UB3LYP-D method in the GAUSSIAN 09 program package. The basis sets are 6-31G++ (O and F) and 6-31G (the other atoms). For the estimation of intermolecular magnetic interaction, we applied our evaluation scheme, which has been studied previously [55].

The Monte Carlo (MC) calculations were performed using a standard Metropolis method. We applied a system size of 256 with periodic boundary conditions; it was subsequently confirmed that there is no size dependence. Each run was performed after discarding the initial 50 000 MC steps per spin (MCS) and the subsequent 450 000 MCS for equilibration.

III. RESULTS

A. Crystal structure and magnetic model

The crystallographic data are summarized in Table I [56]. Figure 1(a) shows the molecular structure of $[Mn(hfac)_2]\cdot(o\text{-Py-V})$, in which a radical center is directly bonded to a Mn ion. Thus, the formation of a Mn-verdazyl hybrid spin is expected through strong coupling via the coordination. The crystal structure at room temperature (RT) is isomorphous to that of $[Zn(hfac)_2]\cdot(o\text{-Py-V})$ [19]. We performed MO calculations to evaluate the intramolecular interaction between spins on Mn^{2+} ($S_{Mn} = 5/2$) and the verdazyl radical ($S_V = 1/2$) as well as the intermolecular interactions between their resultant spins. The intramolecular interaction J_{intra}, which is defined with the spin Hamiltonian as $\mathcal{H} = J_{intra}S_{Mn}S_V$, is evaluated to be approximately 664 K. This strong AF J_{intra} gives rise to a large energy gap of $3J_{intra}$ between the resultant spins of $S = 2$ and 3, as shown in Fig. 1(b). Because the lower states of $S = 2$ are well separated from the excited states of $S = 3$, the $[Mn(hfac)_2]\cdot(o\text{-Py-V})$ molecule can be considered to have a Mn-verdazyl hybrid spin $S = 2$ for $T \ll 3J_{intra}$.

We mainly focus on the structural features related to the *o*-Py-V at 25 K to consider intermolecular interactions in

TABLE I. Crystallographic data for $[Mn(hfac)_2]\cdot(o\text{-Py-V})$.

Parameter	Value	
Formula	$C_{29}H_{18}F_{12}N_5O_4Mn$	
Crystal system	Monoclinic	
Space group	$P2_1/c$	$P2_1$
Temperature (K)	RT	25(2)
Wavelength (Å)	0.7107	
a (Å)	9.029(2)	8.7586(12)
b (Å)	32.307(8)	31.988(5)
c (Å)	10.967(3)	10.8617(15)
β (deg)	93.184(3)	92.568(4)
V (Å^3)	3194.1(14)	3194.1(14)
Z	4	
D_{calc} (g cm^{-3})	1.629	1.712
Total reflections	5260	10584
Reflection used	4378	6429
Parameters refined	460	919
$R\ [I > 2\sigma(I)]$	0.0659	0.0638
$R_w\ [I > 2\sigma(I)]$	0.1805	0.1082
Goodness of fit	1.082	0.926
CCDC	1048586	1048588

low-temperature regions. The MO calculations indicated that approximately 70% of the total spin density of $S = 2$ is present in the Mn atom, whereas the *o*-Py-V has approximately 28% of the total spin density of $S = 2$. Because the hfac functions as a spacer between molecular spins, there is no direct correlation between the Mn atoms. Therefore, the intermolecular magnetic interactions arise through the overlapping of the molecular orbitals on the *o*-Py-V. We evaluated the intermolecular magnetic interactions of all molecular pairs within 4.0 Å at 25 K through the *ab initio* MO calculations. Consequently, we found that there are two types of dominant interactions related to M_0-M_1 and M_0-M_2 molecular pairs, as shown in Fig. 1(c). They have an inversion center between molecules at RT. At 25 K, each molecular pair is composed of two crystallographically independent molecules owing to the disappearance of the inversion center. A strong F interaction J_F is evaluated between molecules labeled M_0 and M_1, as shown in Fig. 1(c). The two N-C short contacts d_1 and d_1' are approximately 3.35 and 3.42 Å, respectively. An AF interaction J_{AF} is evaluated between molecules labeled M_0 and M_2, as shown in Fig. 1(c). The two C-C short contacts d_2 and d_2' are approximately 3.31 and 3.33 Å, respectively. These two molecular pairs are alternately aligned along the c axis, as shown in Fig. 1(c). Thus, the hybrid spins form an F-AF alternating chain consisting of J_F and J_{AF}, in analogy with that for $[Zn(hfac)_2]\cdot(o\text{-Py-V})$ [19], as shown in Fig. 1(d). The values of the interactions are evaluated as $J_F/k_B = -1.21$ K and $J_{AF}/k_B = 0.26$ K ($|J_{AF}/J_F| = 0.21$), which are defined in the spin Hamiltonian given by

$$\mathcal{H} = J_F \sum_i S_{2i}\cdot S_{2i+1} + J_{AF}\sum_i S_i \cdot S_{2i-1} + D\sum_i \left(S_i^z\right)^2 + E\sum_i \left\{\left(S_i^x\right)^2 - \left(S_i^y\right)^2\right\}, \quad (1)$$

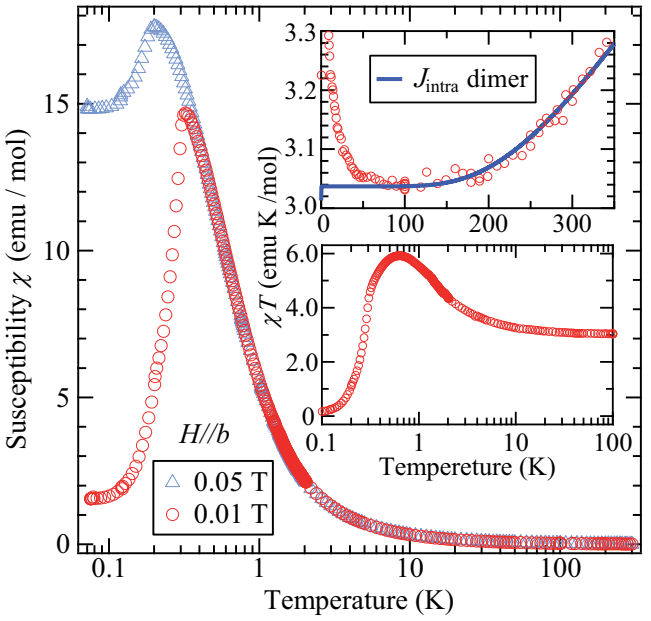

FIG. 2. Temperature dependence of magnetic susceptibility ($\chi = M/H$) of $[Mn(hfac)_2]\cdot(o\text{-Py-V})$ at 0.01 and 0.05 T for $H//b$. The upper and lower insets show the temperature dependence of χT for high- and low-temperature regions, respectively. The solid line represents the calculated results for the S_{Mn}-S_V dimer coupled by J_{intra}.

where D and E are on-site anisotropies; the x-, y-, z-axes correspond to the $-a\sin\beta$, c, and b directions, respectively (discussed later); and S is an $S = 2$ spin operator.

B. Magnetic susceptibility

Figure 2 shows the temperature dependence of magnetic susceptibility ($\chi = M/H$) for $H//b$. The χT decreases with decreasing temperature and becomes approximately constant around 100 K, as shown in the upper inset of Fig. 2. The constant value of χT is very close to the Curie constant of 3.0 emu K/mol for an $S = 2$ noninteracting spin, which evidences the formation of hybrid spin $S = 2$ through the strong AF J_{intra}. We calculated χT for the S_{Mn}-S_V dimer coupled through J_{intra} and obtained an impressive agreement between the experiment and calculation above approximately 100 K by using $J_{intra}/k_B = 325$ K, where we assumed $g_b = 2.02$ and a sample purity of 99%. Below 100 K, χT increases with decreasing temperature until approximately 0.6 K, as shown in the lower inset of Fig. 2. This behavior indicates contributions from strong F interaction and/or large anisotropy, which probably arises from a magnetic dipole-dipole interaction. The Curie-Weiss law, $\chi = C/(T - \theta_W)$, describes the system between 5 and 100 K. The estimated Curie constant and Weiss temperature are approximately $C = 3.01$ emu K/mol and $\theta_W = +0.78(4)$ K, respectively. Below 0.6 K, χT decreases with decreasing temperature, which indicates the additional weak AF interactions. We found distinct sharp peaks in χ at lower temperatures. These peaks are associated with phase transitions to a three-dimensional (3D) order because of weak but finite 3D couplings.

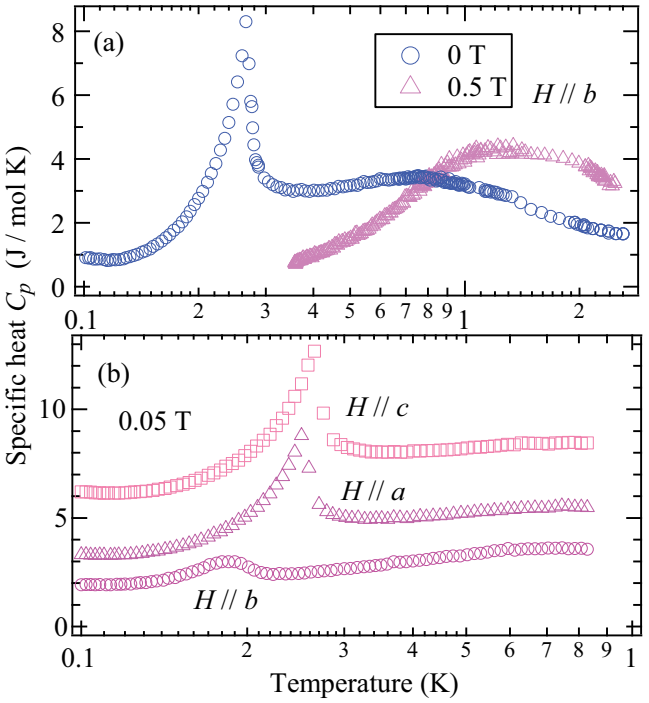

FIG. 3. Specific heat of $[Mn(hfac)_2]\cdot(o\text{-Py-V})$ at (a) 0 and 0.5 T for $H//b$ and (b) 0.05 T for the field parallel to the three crystallographic axes. The values for $H//a$ and $H//c$ have been shifted up by 2.0 and 5.0 J/mol K, respectively.

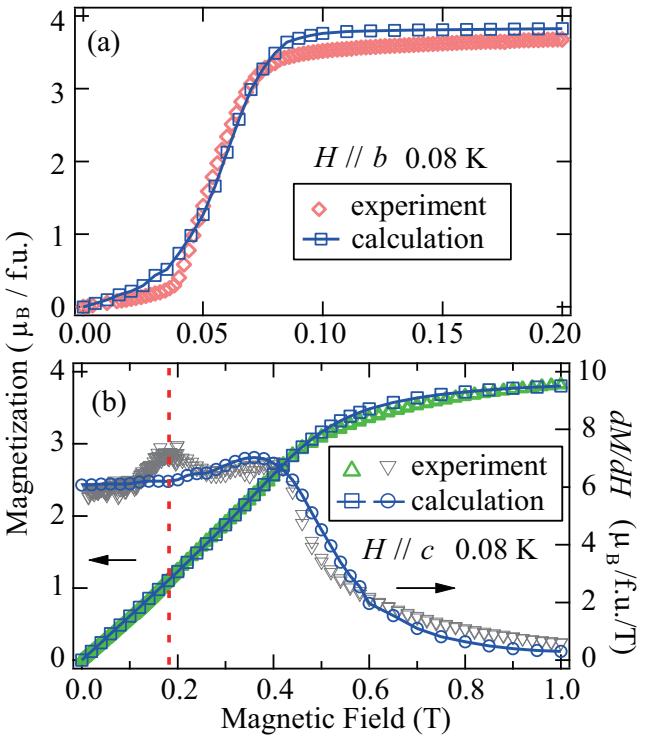

FIG. 4. Magnetization curve of $[Mn(hfac)_2]\cdot(o\text{-Py-V})$ at 0.08 K for (a) $H//b$ and (b) $H//c$. The vertical dashed line shows the field where dM/dH for $H//c$ exhibits the nontrivial peak. The solid lines with symbols represent the results calculated using the MC method.

C. Specific heat

The experimental result for the specific heat C_p at zero field exhibits a λ-type sharp peak associated with the phase transition to the 3D order at $T_N = 0.27$ K, as shown in Fig. 3(a). Although the lattice contributions are not subtracted from C_p, the magnetic contributions are expected to be dominant in the low-temperature regions considered here. Above T_N, we observed a broad peak at approximately 0.8 K, which clearly indicates the development of 1D short-range order in the $S = 2$ alternating chain. By application of the magnetic field, the broad peak shifts to the higher-temperature region, and C_p steeply decreases with decreasing temperature below the peak temperature reflecting the almost fully polarized state with little residual entropy, as shown in Fig 3(a). On the field-direction dependence of C_p at a weak field of 0.05 T, the phase-transition peak exhibits a significant change for $H//b$, whereas there is no remarkable change for $H//a$ and $H//c$, as shown in Fig. 3(b). This result indicates large easy-axis anisotropy along the b axis, as considered in Eq. (1).

D. Magnetization curve

Next, we describe the remarkable behavior of the low-temperature magnetization curves. The measured saturation magnetization $M_{sat} \sim 4.0\mu_B$/f.u. is consistent with that theoretically expected in the $S = 2$ system. We observed a distinct metamagnetic phase transition at $H_c \sim 0.06$ T for $H//b$, which is defined as the middle point of the steep magnetization change. On the other hand, the magnetization curve for $H//c$ apparently exhibits a monotonic increase, as shown in Figs. 4(a) and 4(b). This metamagnetic phase transition demonstrates the presence of large easy-axis anisotropy with the relation $|D| \gg J_{AF}$ if we assume a classical spin system. Furthermore, we found an anomalous peak in the field derivative of magnetization (dM/dH) for $H//c$. It should be noted that the value of magnetization at a peak field of approximately 0.18 T corresponds to $M_{sat}/4 \sim 1.0\mu_B$/f.u.

E. ESR

In order to evaluate the on-site anisotropy, we performed ESR measurements. Figure 5(a) shows the temperature dependence of the resonance fields at 94.3 GHz for $H//a$. In high-temperature regions, the transitions between $S = 2$ states are forbidden because of the large energy gap between the $S = 2$ states and excited $S = 3$ states, as shown in Fig. 1(b). With decreasing temperature, the resonance signals originating from the transitions between $S = 2$ states are enhanced. Considering the energy scale of the interactions and the broad peak temperature of the specific heat, the magnetic correlation length in the chain direction is expected to be quite short at 1.5 K. Therefore, we can consider the observed signals to be the paramagnetic resonance of the hybrid spin $S = 2$. Figures 5(b)–5(d) show the frequency dependence of the resonance fields at 1.5 K for $H//a$, $H//b$, and $H//c$. Each signal is split owing to the slightly different mean fields in two crystallographically independent molecules in the low-temperature crystal structure. We plotted the resonance fields in the frequency-field diagram, as shown in Fig. 6. There are clear differences between the three field directions, which

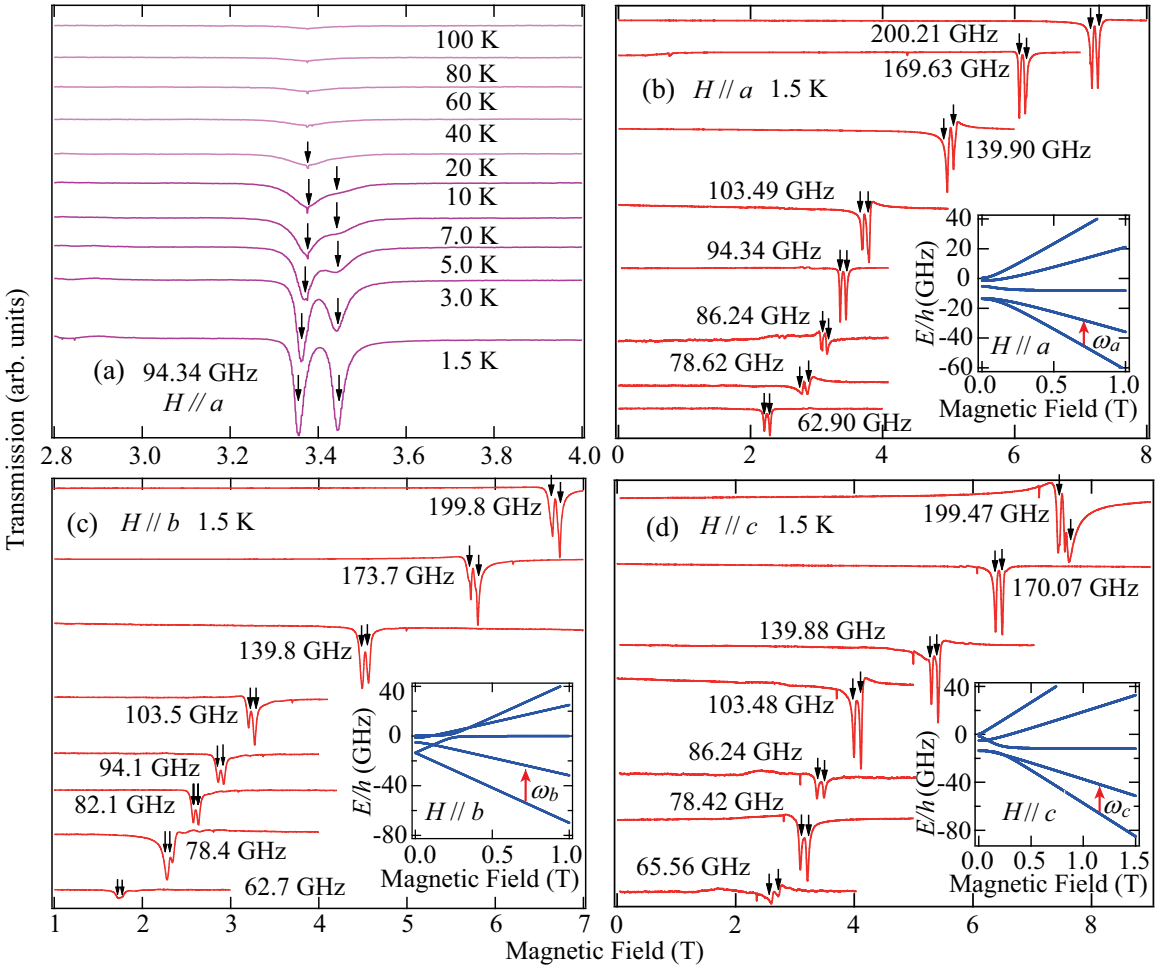

FIG. 5. (a) Temperature dependence and (b)–(d) frequency dependence of ESR absorption spectra of $[Mn(hfac)_2]\cdot(o\text{-Py-V})$ at 94.3 GHz and 1.5 K for (a) and (b) $H//a$, (c) $H//b$, and (d) $H//c$. The arrows indicate the resonance fields. Each inset shows the calculated energy branch.

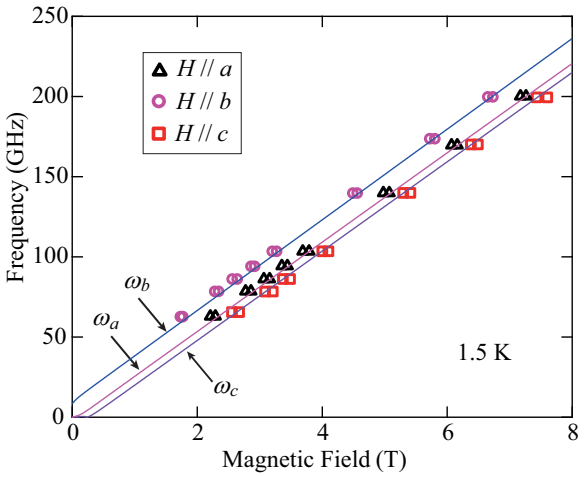

FIG. 6. Frequency-field diagram of the resonance fields at 1.5 K for $H//a$, $H//b$, and $H//c$. The solid lines indicate the calculated paramagnetic resonance modes of the hybrid spin $S = 2$ with on-site biaxial anisotropy, which correspond to the transitions indicated by the arrows in the energy branches.

are much larger than the difference between the split peaks. Therefore, the resonance fields for each direction can be considered to indicate one resonance mode.

IV. ANALYSIS AND DISCUSSION

We evaluate magnetic anisotropy from the frequency dependence of ESR resonance signals. We consider the on-site biaxial anisotropy as follows: $\mathcal{H} = D(S_z)^2 + E\{(S_x)^2 - (S_y)^2\} + g_i\mu_B H S_i$, where μ_B is the Bohr magneton, H is the external magnetic field, and i represents the direction of H. The principal axes are defined in the same manner as in Eq. (1). As shown in Fig. 6, we obtained good agreement between the experimental and calculated results for the resonance modes by using the following parameters: $D/k_B = -0.16$ K, $E/k_B = -0.03$ K, $g_b = 2.02$, and $g_a = g_c = 1.99$. As the ESR measurements were conducted at a sufficiently low temperature of 1.5 K, only the ESR transitions from the ground state are mainly observed. Although energy levels are strongly mixed because of the anisotropy and applied magnetic fields, as shown in the insets of Figs. 5(b)–5(d), the ESR selection rule permits one resonance mode for each field direction at

experimental fields greater than 1T. The resonance modes for $H//a$, $H//b$, and $H//c$ correspond to the transitions ω_a, ω_b, and ω_c indicated by the arrows in the energy branches, respectively. For the easy-axis direction ($H//b$), the ground state and first excited state correspond to $|-2\rangle$ and $|-1\rangle$, where the eigenstates are defined as $|S_z\rangle$, at the experimental fields, respectively.

Finally, we discuss the ground state of the present spin model. As H_c depends only on the value of J_{AF} in a classical spin system, we evaluated $J_{AF}/k_B = 0.04$ K to show a metamagnetic phase transition at H_c. Considering the spin Hamiltonian in Eq. (1), the Weiss temperature is given by $\theta_W = -(2D + J_F + J_{AF})S(S+1)/3k_B$ for $H//b$. Thus, we can roughly evaluate $J_F/k_B = -0.11$ K ($|J_{AF}/J_F| \sim 0.36$) by using the above relation and other parameters. Although the absolute values of J_{AF} and J_F are nearly one order smaller than those expected from the *ab initio* MO calculation, we obtained relatively close values for $|J_{AF}/J_F|$. We calculated the magnetization curves at the experimental temperature for $H//b$ and $H//c$, which correspond to the easy axis and hard axis, respectively, by using the classical MC method with the parameters obtained from Eq. (1), as shown in Figs. 4(a) and 4(b). Assuming the Heisenberg case, the strong interaction J_F in the $S = 2$ F-AF chain is expected to form an $S = 4$ VBS with an extremely small Haldane gap in the same manner as the $S = 1/2$ F-AF chain [50]. In the present case, however, the large anisotropy probably causes such an energy gap to disappear and stabilizes a Néel state. It is noteworthy that the anomalous magnetization at $M_{sat}/4$ for $H//c$ does not appear in the calculated result for the classical case. The quantum $S = 4$ system, which satisfies the necessary condition for realizing a 1/4 magnetization plateau [57], could have a relatively high density of states near the excited state associated with $M_{sat}/4$ owing to the discrete nature of the spin. Therefore, the anomalous magnetization at $M_{sat}/4$ probably originates from the quantum nature of the $S = 2$ F-AF chain with Ising anisotropy.

V. SUMMARY

We have succeeded in synthesizing a Mn-verdazyl complex [Mn(hfac)$_2$]·(*o*-Py-V). Through the analysis of magnetic susceptibility and ESR spectra, we revealed that the strong AF intramolecular interaction between spins on Mn^{2+} and the verdazyl radical forms a hybrid spin $S = 2$ below about 100 K. The *ab initio* MO calculation and experimental results evidenced the first realization of an $S = 2$ F-AF alternating chain with Ising anisotropy. Furthermore, we observed an anomalous change in the magnetization at 1/4 of the saturation value, which possibly originates from the quantum nature of the present spin model. Consequently, we demonstrated the realization of an unprecedented type of $S > 1$ spin system by using the metal-radical hybrid-spin approach. The present results provide a way to realize a variety of unconventional spin systems with different types of spin size and anisotropy and will stimulate studies on unexplored $S > 1$ spin systems. The hybrid-spin approach on verdazyl-based materials is potentially capable of manipulating all the essential parameters for designing magnetic materials such as spin size, magnetic anisotropy, and magnetic interaction.

ACKNOWLEDGMENTS

We thank T. Tonegawa, K. Okamoto, T. Okubo, and T. Shimokawa for the valuable discussions. This research was partly supported by Grant for Basic Science Research Projects from the Sumitomo Foundation, the Shorai Foundation for Science and Technology, and KAKENHI (Grants No. 24540347 and No. 24340075). Part of this work was performed under the interuniversity cooperative research program of the joint-research program of ISSP, the University of Tokyo, and the Institute for Molecular Science.

[1] H. Nishide and K. Oyaizu, Science **319**, 737 (2008).
[2] Y. Morita, S. Nishide, T. Murata, M. Moriguchi, A. Ueda, M. Satoh, K. Arifuku, K. Sato, and T. Takui, Nat. Mater. **10**, 947 (2011).
[3] P. Coronado and P. Day, Chem. Rev. **104**, 5419 (2004).
[4] T. Sugawara, H. Komatsu, and K. Suzuki, Chem. Soc. Rev. **40**, 3105 (2011).
[5] M. Takahashi, P. Turek, Y. Nakazawa, M. Tamura, K. Nozawa, D. Shiomi, M. Ishikawa, and M. Kinoshita, Phys. Rev. Lett. **67**, 746 (1991).
[6] E. V. Tretyakov and V. I. Ovcharenko, Russ. Chem. Rev. **78**, 971 (2009).
[7] H. Yamaguchi, K. Iwase, T. Ono, T. Shimokawa, H. Nakano, Y. Shimura, N. Kase, S. Kittaka, T. Sakakibara, T. Kawakami, and Y. Hosokoshi, Phys. Rev. Lett. **110**, 157205 (2013).
[8] H. Yamaguchi, T. Okubo, K. Iwase, T. Ono, Y. Kono, S. Kittaka, T. Sakakibara, A. Matsuo, K. Kindo, and Y. Hosokoshi, Phys. Rev. B **88**, 174410 (2013).
[9] H. Yamaguchi, H. Miyagai, T. Shimokawa, K. Iwase, T. Ono, Y. Kono, N. Kase, K. Araki, S. Kittaka, T. Sakakibara, T. Kawakami, K. Okunishi, and Y. Hosokoshi, J. Phys. Soc. Jpn. **83**, 033707 (2014).
[10] H. Yamaguchi, T. Okubo, S. Kittaka, T. Sakakibara, K. Araki, K. Iwase, N. Amaya, T. Ono, and Y. Hosokoshi, Sci. Rep. **5**, 15327 (2015).
[11] K. Katoh, Y. Hosokoshi, K. Inoue, and T. Goto, J. Phys. Soc. Jpn. **69**, 1008 (2000).
[12] Y. Hosokoshi, K. Katoh, Y. Nakazawa, H. Nakano, and K. Inoue, J. Am. Chem. Soc. **123**, 7921 (2001).
[13] J. Laugier, P. Rey, C. Benelli, D. Gatteschi, and C. Zanchini, J. Am. Chem. Soc. **108**, 6931 (1986).
[14] K. Inoue, T. Hayamizu, H. Iwamura, D. Hashizumi, and Y. Ohashi, J. Am. Chem. Soc. **118**, 1803 (1996).
[15] C. Train, L. Norel, and M. Baumgarten, Coord. Chem. Rev. **253**, 2342 (2009).
[16] B. D. Koivisto and R. G. Hicks, Coord. Chem. Rev. **249**, 2612 (2005).
[17] C. W. Johnston, S. D. J. McKinnon, B. O. Patrick, and R. G. Hicks, Dalton Trans. **42**, 16829 (2013).
[18] D. J. R. Brook, V. Lynch, C. Conklin, and M. A. Fox, J. Am. Chem. Soc. **119**, 5155 (1997).
[19] H. Yamaguchi, Y. Shinpuku, T. Shimokawa, K. Iwase, T. Ono, Y. Kono, S. Kittaka, T. Sakakibara, and Y. Hosokoshi, Phys. Rev. B **91**, 085117 (2015).

[20] D.-Z. Gao, Y.-Q. Sun, D.-Z. Liao, Z.-H. Jiang, and S.-P. Yan, Z. Anorg. Allg. Chem. **634**, 1950 (2008).
[21] A. Okazawa, Y. Nagaichi, T. Nogami, and T. Ishida, Inorg. Chem. **47**, 8859 (2008).
[22] A. Okazawa and T. Ishida, Inorg. Chem. **49**, 10144 (2010).
[23] F. D. M. Haldane, Phys. Rev. Lett. **50**, 1153 (1983).
[24] S. Todo and K. Kato, Phys. Rev. Lett. **87**, 047203 (2001).
[25] H. Nakano and A. Terai, J. Phys. Soc. Jpn. **78**, 014003 (2009).
[26] K. Katsumata, H. Hori, T. Takeuchi, M. Date, A. Yamagishi, and J. P. Renard, Phys. Rev. Lett. **63**, 86 (1989).
[27] I. A. Zaliznyak, S.-H. Lee, and S. V. Petrov, Phys. Rev. Lett. **87**, 017202 (2001).
[28] I. Affleck, T. Kennedy, E. H. Lieb, and H. Tasaki, Phys. Rev. Lett. **59**, 799 (1987).
[29] M. Hagiwara, K. Katsumata, I. Affleck, B. I. Halperin, and J. P. Renard, Phys. Rev. Lett. **65**, 3181 (1990).
[30] S. Itoh, H. Tanaka, and M. J. Bull, J. Phys. Soc. Jpn. **71**, 1148 (2002).
[31] G. E. Granroth, M. W. Meisel, M. Chaparala, Th. Jolicoeur, B. H. Ward, and D. R. Talham, Phys. Rev. Lett. **77**, 1616 (1996).
[32] C. Stock, L. C. Chapon, O. Adamopoulos, A. Lappas, M. Giot, J. W. Taylor, M. A. Green, C. M. Brown, and P. G. Radaelli, Phys. Rev. Lett. **103**, 077202 (2009).
[33] T. Birk, K. S. Pedersen, S. Piligkos, C. Aa. Thuesen, H. Weihe, and J. Bendix, Inorg. Chem. **50**, 5312 (2011).
[34] M. B. Stone, G. Ehlers, and G. E. Granroth, Phys. Rev. B **88**, 104413 (2013).
[35] S. Itho, T. Yokoo, S. Yano, D. Kawana, H. Tanaka, and Y. Endoh, J. Phys. Soc. Jpn. **81**, 084706 (2012).
[36] H. J. Schulz, Phys. Rev. B **34**, 6372 (1986).
[37] M. Oshikawa, J. Phys.: Condens. Matter **4**, 7469 (1992).
[38] H. Aschauer and U. Schollwöck, Phys. Rev. B **58**, 359 (1998).
[39] T. Tonegawa, K. Okamoto, H. Nakano, T. Sakai, K. Nomura, and M. Kaburagi, J. Phys. Soc. Jpn. **80**, 043001 (2011).
[40] K. Okamoto, T. Tonegawa, H. Nakano, T. Sakai, K. Nomura, and M. Kaburagi, J. Phys.: Conf. Ser. **302**, 012014 (2011).
[41] K. Okamoto, T. Tonegawa, T. Sakai, and M. Kaburagi, JPS Conf. Proc. **3**, 014022 (2014).
[42] Y.-C. Tzeng, Phys. Rev. B **86**, 024403 (2012).
[43] J. A. Kjäll, M. P. Zaletel, R. S. K. Mong, J. H. Bardarson, and F. Pollmann, Phys. Rev. B **87**, 235106 (2013).
[44] M. Yamanaka, M. Oshikawa, and S. Miyashita, J. Phys. Soc. Jpn. **65**, 1562 (1996).
[45] M. Nakamura and S. Todo, Phys. Rev. Lett. **89**, 077204 (2002).
[46] A. Kitazawa and K. Nomura, J. Phys. Soc. Jpn. **66**, 3379 (1997).
[47] T. Sakai, J. Phys. Soc. Jpn. **64**, 251 (1995).
[48] S. Watanabe and H. Yokoyama, J. Phys. Soc. Jpn. **68**, 2073 (1999).
[49] S. Kokado and N. Suzuki, J. Phys. Soc. Jpn. **68**, 3091 (1999).
[50] K. Hida, Phys. Rev. B **45**, 2207 (1992).
[51] K. Hida, J. Phys. Soc. Jpn. **62**, 1463 (1993).
[52] K. Hida, J. Phys. Soc. Jpn. **67**, 1416 (1998).
[53] M. C. Burla, R. Caliandro, M. Camalli, B. Carrozzini, G. L. Cascarano, L. De Caro, C. Giacovazzo, G. Polidori, and R. Spagna, J. Appl. Crystallogr. **38**, 381 (2005).
[54] G. M. Sheldrick, SHELXL97, program for crystal structure determination (University of Göttingen, Göttingen, Germany, 1997).
[55] M. Shoji, K. Koizumi, Y. Kitagawa, T. Kawakami, S. Yamanaka, M. Okumura, and K. Yamaguchi, Chem. Phys. Lett. **432**, 343 (2006).
[56] Crystallographic data have been deposited with the Cambridge Crystallographic Data Centre, Deposition No. CCDC 1048586 for RT and CCDC 1048588 for 25 K.
[57] M. Oshikawa, M. Yamanaka, and I. Affleck, Phys. Rev. Lett. **78**, 1984 (1997).